Mineralogical Magazine, December 2007, Vol. 71(6), pp. 651–669

Amphiboles from the Kola Superdeep Borehole: Fe^{3+} contents from crystal-chemical analysis and Mössbauer spectroscopy

Y. Uvarova[1], E. Sokolova[1,3], F. C. Hawthorne[1,*], C. A. McCammon[2], V. I. Kazansky[3,†] and K. V. Lobanov[3]

[1] Department of Geological Sciences, University of Manitoba Winnipeg, Manitoba, Canada R3T 2N2
[2] Bayerisches Geoinstitut, Universität Bayreuth, D-95440 Bayreuth, Germany
[3] Institute of the Geology of Ore Deposits, Petrography, Mineralogy and Geochemistry, Russian Academy of Sciences, Staromonetny 35, 119017 Moscow, Russia

[*Received 18 March 2008; Accepted* 23 May 2008]

ABSTRACT

The crystal structures of a suite of amphiboles from the Kola Superdeep Borehole, Russia, have been refined to *R* values of ~3% using single-crystal Mo-*K*α X-ray diffraction data. The same crystals used in the collection of the intensity data were subsequently analysed by electron microprobe (EMP) and milliprobe Mössbauer spectroscopy. Site populations were assigned from the results of site-scattering refinement and stereochemical analysis, taking into account the unit formula determined for each crystal. The $Fe^{3+}/(Fe^{2+}+Fe^{3+})$ values were derived (1) by least-squares refinement of the Mössbauer spectra, and (2) SREF (Structure REFinement) by careful analysis of the mean bond lengths at the *M*(2) site using two possible models for the behaviour of Ti^{4+}: (i) Ti^{4+} at *M*(2); and (ii) Ti^{4+} at *M*(1). The agreement between the SREF and Mössbauer/EMP values for Fe^{3+} is very close for Ti^{4+} assigned to *M*(2). This result indicates that the calculation of Fe^{3+} contents in amphiboles from refined site populations and <*M*(2)–O> distances are accurate. This paper presents the first confirmation of this result.

Keywords: amphibole, crystal-structure refinement, electron microprobe analysis, Mössbauer spectroscopy, Kola Superdeep Borehole.

Introduction

The Kola Superdeep Borehole (Kola S.D.B.) provides a continuous 12.2 km section through the rocks of the Pechenga District of the Baltic Shield, penetrating the Proterozoic-Archaean boundary at a depth of ~6.8 km (Kazansky, 1992, 1997; Kazansky *et al.*, 2002; Isanina *et al.*, 2000). The Proterozoic rocks consist of metavolcanic and metasedimentary rocks down to 6.8 km, and are underlain by Archaean gneisses and amphibolites. Earlier studies showed that amphibole is present in nearly all rocks sampled from the borehole and is commonly accompanied by biotite and feldspar (e.g. Nikitina *et al.*, 2002). Moreover, surface analogues of the rocks in the borehole have been identified (Lobanov *et al.*, 2002), and comparison of the major- and trace-element, isotopic and textural characteristics of these surface analogues with the rocks recovered from the borehole will provide unique insight into the effects of near-surface alteration. We are currently involved in a detailed mineralogical, petrological and geochemical study of these unique samples.

The analysis of FeO and Fe_2O_3 in amphiboles

The analysis of FeO and Fe_2O_3 is still a major impediment to adequate characterization of rock-forming minerals. Despite improvements in wet-chemical analysis techniques, 30 mg of pure mineral separate is needed for analyses of adequate accuracy. Mössbauer spectroscopy is

* E-mail: frank_hawthorne@umanitoba.ca
† kazansky@igem.ru
DOI: 10.1180/minmag.2007.071.6.651

probably the instrumental technique of choice, but this still involves many milligrams of pure mineral separate, and for many parageneses, this is an impractical constraint. Milli-beam methods are available for the determination of $Fe^{3+}/(Fe^{2+}+Fe^{3+})$: (1) Milli-Mössbauer spectroscopy (McCammon, 1994); (2) Milli-XANES (X-ray absorption near-edge structure) (Delaney *et al.*, 1996; Dyar *et al.*, 2002); (3) EELS (electron energy loss spectroscopy) - ELNES (energy loss near-edge spectroscopy) (Garvie and Buseck, 1998; Garvie *et al.*, 2004; van Aken *et al.*, 1998; van Aken and Liebscher, 2002). For these techniques, there are few experimental facilities. Hence, until the instrumentation becomes widespread, they are not generally viable methods for routine determination of $Fe^{3+}/(Fe^{2+}+Fe^{3+})$ in petrological studies. An alternative approach is the Flank method that optimizes the use of an electron microprobe (EMP) to use X-ray spectroscopy to determine Fe^{2+}/Fe^{3+} ratios via the positions and intensities of the FeL_{α} and FeL_{β} peaks as a function of valence state (Höfer *et al.*, 1994). Enders *et al.* (2000) have tested this method extensively for sodic amphiboles and have shown that it can be reasonably accurate down to an FeO(total) content of 6–8 wt.%. However, they also stated that the calibration procedures are particularly laborious and complicated, suggesting that it is not ideal as a routine method for Fe^{2+}/Fe^{3+} determination.

For amphiboles, it is critical that Fe^{2+}/Fe^{3+} be determined on a routine basis. For many years progress in amphibole crystal chemistry has required accurate determination of Fe^{2+}/Fe^{3+} ratios, and this requirement is now also essential for petrological studies (Martin, 2007; Schumacher, 2007). Indeed, determination of Fe^{2+}/Fe^{3+} ratios has long been considered essential for work on kaersutite and their associated rocks (e.g. Dyar *et al.*, 1992, 1993; King *et al.*, 1999; Popp *et al.*, 1995, 2006). Amphibole crystal chemistry and crystal-structure refinement, combined with accurate electron microprobe analysis (EMPA), may provide sufficient information for Fe^{3+} contents of amphiboles to be determined stereochemically (e.g. Hawthorne *et al.*, 1993, 1994, 1998; Oberti *et al.*, 1995*a*,*b*). However, there has not as yet been any independent verification of Fe^{3+} contents of amphiboles derived in this manner.

We are currently characterizing the amphiboles from the rocks of the Kola Superdeep Borehole by crystal-structure refinement in order to derive accurate site-populations. This provides an ideal opportunity to test the accuracy of crystal-chemical analysis as a method of determining the Fe^{3+} contents of amphiboles, as extremely accurate chemical compositions of the constituent amphiboles are required, and a combined SREF-Milli-Mössbauer study was deemed appropriate. The results of this investigation are presented here. The crystal structure of *C*2/*m* amphibole is shown in Fig. 1, and will be referred to extensively in the following text.

Experimental

Borehole samples and the amphibole-type each contains are listed in Table 1. Fragments of the drill core were crushed gently to disaggregate the mineral grains, and amphibole crystals were

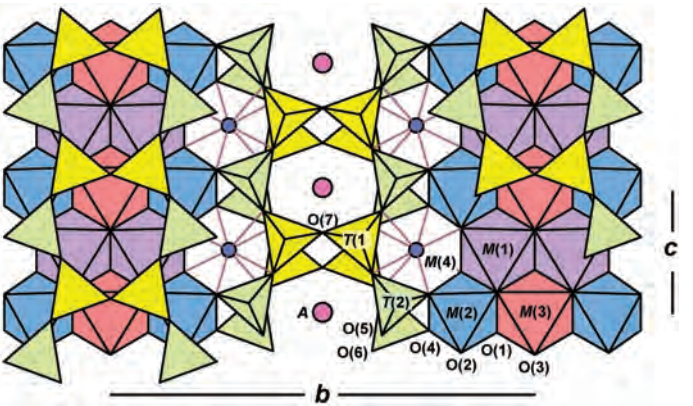

FIG. 1. The *C*2/*m* amphibole structure projected onto (100); polyhedra: *T*(1) = yellow, *T*(2) = pale green, *M*(1) = mauve, *M*(2) = blue, *M*(3) = pink; sites: *M*(4) = blue circle, *A* = fuchsia circle.

TABLE 1. The Kola amphiboles and rocks in which they occur.

Sample*	Amphibole name	Rock type
K-4967	Ferrotschermakite	Amphibole-magnetite-ilmenite schist
K-6452.2	Magnesiohornblende	Schistose epidote-titanite-bearing amphibolite
K-6600	Magnesiohornblende	Schistose epidote-titanite-bearing amphibolite
K-6946	Magnesiohornblende	Titanite-bearing hornblende amphibolite
K-7277.2	Magnesiohornblende	Titanite-bearing hornblende amphibolite
K-7536	Hastingsite	Titanite-bearing hornblende amphibolite
K-7681.2	Magnesiohornblende	Titanite-bearing hornblende amphibolite
K-8451	Edenite	Epidote-biotite-hornblende amphibolite
K-8746.2	Hastingsite	Epidote-biotite-hornblende amphibolite
K-8858	Ferro-edenite	Titanite-bearing hornblende amphibolite
K-9083.2	Hastingsite	Titanite-bearing hornblende amphibolite
K-9264.8	Magnesiohornblende	Biotite-hornblende amphibolite
K-9940.3	Ferropargasite	Epidote-biotite-hornblende amphibolite
K-10504.5	Magnesiohornblende	Epidote-biotite-hornblende amphibolite
K-11345	Magnesiohornblende	Titanite-bearing hornblende amphibolite
K-11468.3–11523.3	Magnesiohornblende	Epidote-biotite-hornblende amphibolite
K-12234.5–12261.5	Edenite	Biotite-hornblende amphibolite

* The numerical part of the sample number gives the depth below the surface in metres.

selected for diffraction work on the basis of size, optical clarity and lack of alteration. Each crystal was attached to the tip of a tapered glass fibre and mounted on a goniometer head.

X-ray data collection

Crystals were mounted on a BRUKER *P*4 four-circle diffractometer equipped with monochromatic Mo-$K\alpha$ radiation and an APEX 4K CCD area detector. Reflection intensities were collected to ~60.00º2θ using 15 s per 0.2º frame with a crystal-to-detector distance of 4 cm. Empirical absorption corrections (SADABS; Sheldrick, 1998) were applied. Unit-cell parameters were obtained by least-squares refinement from the positions of ~3000 reflections with $I > 10\sigma I$. Unit-cell parameters, *R* indices and other information pertinent to data collection and crystal-structure refinement are given in Table 2.

Crystal-structure refinement

All calculations were done with the SHELXTL PC (Plus) system of programs by full-matrix least-squares on F^2 using fixed weights proportional to $1/\sigma F^2$. The *R* indices are of the form given in Table 2 and are expressed as percentages. Using ionized scattering factors, all structures refined rapidly in space group *C*2/*m* to *R* indices of ~3% for a model with anisotropic-displacement parameters for all sites except *A*(*m*) and *A*(2). Selected interatomic distances and angles are given in Table 3, and the refined site-scattering values are listed in Table 4. Final atom coordinates and anisotropic-displacement parameters have been deposited with the Principal Editor of *Mineralogical Magazine* and are available from www.minersoc.org/pages/e_journals/dep_mat.html.

EMP analysis

The crystals used in the collection of the X-ray intensity data were mounted in epoxy and placed in small holes of 1" (25 mm) plastic discs, polished and carbon-coated. The EMP analysis was done on a fully automated Cameca SX50 instrument operating in wavelength dispersive spectroscopy mode with the following conditions: excitation voltage 15 kV, specimen current 20 nA, peak count-time 20 s, background count-time 10 s. The following standards and crystals were used for $K\alpha$ X-ray lines: Al: kyanite, TAP; Fe: fayalite, LiF; Si: diopside, PET; Mg: diopside, TAP; Mn: tephroite, LiF; Ti: titanite, LiF; F: fluororiebeckite, TAP. Each grain was analysed on a minimum of ten points to check for

TABLE 2. Crystal data and structure refinement for the Kola amphiboles.

	K-4967	K-6452.2	K-6600	K-6946	K-7277.2	K-7536
a (Å)	9.825(1)	9.8393(5)	9.849(1)	9.8364(5)	9.8727(5)	9.8691(6)
b (Å)	18.108(2)	18.0820(9)	18.090(2)	18.080(1)	18.113(1)	18.114(1)
c (Å)	5.3301(5)	5.3003(3)	5.3186(6)	5.3218(3)	5.3123(3)	5.3253(3)
β (º)	104.910(2)	104.792(1)	104.929(3)	104.927(2)	104.911(1)	105.011(1)
V (Å^3)	916.3(3)	911.8(1)	915.6(3)	914.5(1)	918.0(1)	919.5(2)
Z	2	2	2	2	2	2
Space group	*C*2/*m*	*C*2/*m*	*C*2/*m*	*C*2/*m*	*C*2/*m*	*C*2/*m*
Absorption coefficient (mm^{-1})	3.41	2.55	3.00	4.48	2.96	3.31
F(000)	972.3	931.9	952.1	1028.3	950.3	969.6
$D_{calc.}$ (g/cm^3)	3.301	3.150	3.221	3.521	3.204	3.278
Crystal size (mm)	0.14 × 0.06 × 0.02	0.10 × 0.06 × 0.04	0.10 × 0.06 × 0.04	0.10 × 0.07 × 0.04	0.10 × 0.06 × 0.04	0.14 × 0.04 × 0.04
Radiation/filter	Mo-*K*α/graphite					
2θ-range for data collection (º)	60.04	59.99	60.02	59.99	59.98	60.01
R_{int} (%)	2.43	1.53	4.95	1.58	1.48	2.01
Reflections collected	6347	6316	5374	6348	6338	6401
Independent reflections $F_o > 4\sigma F_o$	1389 1318	1380 1319	1377 935	1381 1315	1383 1362	1388 1300
Refinement method	Full-matrix least squares on F^2, fixed weights proportional to $1/\sigma F_o^2$					
Goodness-of-fit on F^2	1.305	1.104	0.952	1.141	1.343	1.091
Final R_{obs} (%) [$F_o > 4\sigma F_o$]	*R*1 = 5.31	*R*1 = 2.90	*R*1 = 3.80	*R*1 = 2.75	*R*1 = 3.29	*R*1 = 2.66
R indices (all data) (%)	*R*1 = 5.61 *wR*2 = 11.94	*R*1 = 3.05 *wR*2 = 7.20	*R*1 = 7.12 *wR*2 = 8.85	*R*1 = 2.93 *wR*2 = 6.69	*R*1 = 3.33 *wR*2 = 7.48	*R*1 = 2.90 *wR*2 = 6.82

	K-7681.2	K-8451	K-8746.2	K-8858	K-9083.2	K-9264.8
a (Å)	9.8545(8)	9.8426(4)	9.8887(6)	9.8795(5)	9.892(1)	9.8591(5)
b (Å)	18.102(1)	18.0900(8)	18.132(1)	18.120(1)	18.150(2)	18.1015(8)
c (Å)	5.3229(4)	5.3232(2)	5.3345(3)	5.3286(3)	5.3345(6)	5.3117(3)
β (º)	104.921(2)	104.885(1)	105.050(1)	105.020(1)	105.038(2)	104.897(1)
V (Å^3)	917.5(2)	916.0(1)	923.7(2)	921.3(1)	924.9(3)	916.1(1)
Z	2	2	2	2	2	2
Space group	*C*2/*m*	*C*2/*m*	*C*2/*m*	*C*2/*m*	*C*2/*m*	*C*2/*m*
Absorption coefficient (mm^{-1})	3.01	3.16	3.66	3.29	3.70	2.84
F(000)	951.6	963.1	986.6	969.0	987.5	944.9
$D_{calc.}$ (g/cm^3)	3.213	3.264	3.331	3.269	3.332	3.189

Crystal size (mm)	$0.12 \times 0.04 \times 0.04$	$0.20 \times 0.08 \times 0.06$	$0.14 \times 0.06 \times 0.06$	$0.20 \times 0.10 \times 0.06$	$0.20 \times 0.08 \times 0.06$	$0.10 \times 0.06 \times 0.04$
Radiation/filter	Mo-$K\alpha$/graphite					
2θ-range for data collection (°)	59.97	59.99	60.00	59.97	59.92	59.94
R_{int} (%)	2.28	1.46	1.58	2.41	4.05	1.71
Reflections collected	6377	6090	6360	5384	5471	6343
Independent reflections $F_o > 4\sigma F_o$	1385 1215	1384 1326	1393 1277	1383 1146	1384 1005	1381 1356
Refinement method	Full-matrix least squares on F^2, fixed weights proportional to $1/\sigma F_o^2$					
Goodness-of-fit on F^2	1.084	1.088	1.042	1.040	0.974	1.254
Final R_{obs} (%) [$F_o > 4\sigma F_o$]	$R1 = 3.80$	$R1 = 2.47$	$R1 = 2.38$	$R1 = 2.60$	$R1 = 3.41$	$R1 = 3.14$
R indices (all data) (%)	$R1 = 4.40$ $wR2 = 10.07$	$R1 = 2.55$ $wR2 = 6.48$	$R1 = 2.58$ $wR2 = 6.66$	$R1 = 3.44$ $wR2 = 7.24$	$R1 = 5.47$ $wR2 = 8.60$	$R1 = 3.19$ $wR2 = 6.81$

	K-9940.3	K-10504.5	K-11345	K-11468.3–11523.3	K-12234.5–12261.5
a (Å)	9.8621(6)	9.8428(5)	9.8721(5)	9.8387(4)	9.8974(5)
b (Å)	18.105(1)	18.082(1)	18.0902(9)	18.0766(7)	18.1279(9)
c (Å)	5.3290(3)	5.3179(3)	5.3199(3)	5.3239(2)	5.3230(3)
β (°)	104.994(2)	104.922(1)	104.997(1)	104.929(1)	104.992(1)
V (Å^3)	919.1(2)	914.6(1)	917.7(1)	914.9(1)	922.5(1)
Z	2	2	2	2	2
Space group	$C2/m$	$C2/m$	$C2/m$	$C2/m$	$C2/m$
Absorption coefficient (mm^{-1})	3.37	2.96	2.93	2.97	4.44
F(000)	971.2	950.2	953.3	953.1	1026.3
$D_{calc.}$ (g/cm^3)	3.288	3.218	3.217	3.229	3.487
Crystal size (mm)	$0.10 \times 0.02 \times 0.02$	$0.12 \times 0.08 \times 0.06$	$0.14 \times 0.06 \times 0.04$	$0.20 \times 0.08 \times 0.08$	$0.08 \times 0.04 \times 0.02$
Radiation filter	Mo-$K\alpha$/ graphite				
2θ-range for data collection (°)	60.00	60.00	59.38	59.97	60.00
R_{int} (%)	1.94	1.42	1.31	1.83	1.65
Reflections collected	6379	6296	6202	6462	6361
Independent reflections $F_o > 4\sigma F_o$	1388 1329	1381 1357	1346 1331	1379 1332	1393 1362
Refinement method	Full-matrix least squares on F^2, fixed weights proportional to $1/\sigma F_o^2$				
Goodness-of-fit on F^2	1.132	1.169	1.327	1.139	1.196
Final R_{obs} (%) [$F_o > 4\sigma F_o$]	$R1 = 3.36$	$R1 = 2.59$	$R1 = 2.94$	$R1 = 2.45$	$R1 = 2.75$
R indices (all data) (%)	$R1 = 3.53$ $wR2 = 7.95$	$R1 = 2.65$ $wR2 = 6.37$	$R1 = 2.97$ $wR2 = 6.76$	$R1 = 2.51$ $wR2 = 6.54$	$R1 = 2.82$ $wR2 = 6.52$

TABLE 3. Selected interatomic distances (Å) and angles (º) for the Kola amphiboles*.

		K-4967	K-6452.2	K-6600	K-6946	K-7277.2	K-7536	K-7681.2	K-8451	K-8746.2
T(1)−O(1)		1.662	1.628	1.649	1.653	1.635	1.658	1.648	1.654	1.666
T(1)−O(5)		1.681	1.654	1.662	1.674	1.665	1.680	1.671	1.675	1.688
T(1)−O(6)		1.677	1.651	1.669	1.668	1.657	1.674	1.668	1.671	1.682
T(1)−O(7)		1.646	1.631	1.639	1.645	1.636	1.650	1.642	1.648	1.657
<*T*(1)−O>		1.667	1.641	1.655	1.660	1.648	1.666	1.657	1.662	1.673
T(2)−O(2)		1.632	1.621	1.631	1.629	1.623	1.631	1.629	1.631	1.632
T(2)−O(4)		1.609	1.595	1.600	1.605	1.598	1.606	1.607	1.606	1.607
T(2)−O(5)		1.640	1.651	1.649	1.647	1.648	1.647	1.649	1.647	1.645
T(2)−O(6)		1.657	1.668	1.662	1.662	1.668	1.662	1.665	1.661	1.659
<*T*(2)−O>		1.635	1.634	1.636	1.636	1.634	1.637	1.638	1.636	1.636
M(1)−O(1)	×2	2.065	2.069	2.066	2.067	2.072	2.065	2.067	2.067	2.066
M(1)−O(2)	×2	2.158	2.112	2.130	2.147	2.125	2.150	2.138	2.143	2.164
M(1)−O(3)	×2	2.117	2.105	2.109	2.116	2.113	2.108	2.113	2.112	2.121
<*M*(1)−O>		2.113	2.095	2.102	2.110	2.103	2.108	2.106	2.107	2.117
M(2)−O(1)	×2	2.045	2.106	2.072	2.054	2.098	2.068	2.075	2.067	2.051
M(2)−O(2)	×2	2.048	2.076	2.061	2.051	2.082	2.065	2.061	2.057	2.061
M(2)−O(4)	×2	1.954	1.992	1.973	1.956	1.984	1.967	1.970	1.962	1.960
<*M*(2)−O>		2.016	2.058	2.035	2.020	2.055	2.033	2.035	2.029	2.024
M(3)−O(1)	×4	2.124	2.091	2.109	2.117	2.103	2.114	2.112	2.113	2.129
M(3)−O(3)	×2	2.102	2.078	2.097	2.097	2.090	2.101	2.093	2.097	2.109
<*M*(3)−O>		2.117	2.087	2.105	2.110	2.099	2.110	2.106	2.108	2.122
M(4)−O(2)	×2	2.411	2.397	2.407	2.405	2.403	2.410	2.412	2.405	2.415
M(4)−O(4)	×2	2.334	2.317	2.328	2.330	2.331	2.335	2.332	2.324	2.340
M(4)−O(5)	×2	2.664	2.730	2.696	2.673	2.721	2.676	2.687	2.680	2.664
M(4)−O(6)	×2	2.528	2.548	2.542	2.533	2.543	2.544	2.538	2.545	2.542
<*M*(4)−O>		2.484	2.498	2.493	2.485	2.500	2.491	2.492	2.489	2.490
A(2/*m*)−O(5)	×4	3.044	3.003	3.023	3.033	3.018	3.043	3.031	3.035	3.055
A(2/*m*)−O(6)	×4	3.152	3.150	3.146	3.148	3.157	3.129	3.149	3.141	3.144
A(2/*m*)−O(7)	×2	2.521	2.494	2.510	2.516	2.517	2.510	2.513	2.493	2.529
<*A*(2/*m*)−O>		2.983	2.960	2.970	2.976	2.973	2.971	2.975	2.969	2.985
A(*m*)−O(5)	×2	3.052	3.009	3.023	3.031	3.011	3.028	3.015	3.030	3.043
A(*m*)−O(5)	×2	3.140	3.115	3.053	3.130	3.133	3.158	3.159	3.136	3.143
A(*m*)−O(6)	×2	2.767	2.743	2.932	2.780	2.766	2.763	2.753	2.770	2.813
A(*m*)−O(7)		2.495	2.469	2.461	2.501	2.508	2.521	2.533	2.484	2.522
A(*m*)−O(7)		2.670	2.658	2.594	2.644	2.653	2.620	2.629	2.619	2.628
A(*m*)−O(7)		3.188	3.139	3.428	3.214	3.168	3.215	3.184	3.228	3.280
<*A*(*m*)−O>		2.919	2.889	2.944	2.916	2.905	2.917	2.911	2.911	2.936
A(2)−O(5)	×2	2.623	2.594	2.606	2.619	2.818	2.620	2.647	2.605	2.640
A(2)−O(6)	×2	2.814	2.822	2.811	2.815	2.993	2.799	2.840	2.797	2.809
A(2)−O(7)	×2	2.575	2.548	2.565	2.570	2.529	2.566	2.560	2.552	2.583
<*A*(2)−O>		2.671	2.655	2.661	2.668	2.780	2.662	2.682	2.651	2.677
T(1)−O(5)−*T*(2)		134.5	135.62	135.1	134.55	135.6	134.69	134.8	134.62	134.46
T(1)−O(6)−*T*(2)		140.1	138.88	139.4	139.60	138.9	138.96	139.3	139.32	139.14
T(1)−O(7)−*T*(1)		141.9	140.1	140.8	141.2	140.2	140.3	140.8	140.3	140.8
T(1)−*T*(2)−*T*(1)		118.7	118.5	118.6	118.6	118.5	118.6	118.7	118.7	118.6
T(2)−*T*(1)−*T*(1)		120.2	120.4	120.3	120.3	120.4	120.3	120.3	120.3	120.3

Table 3. (*Cont.*)

		K-8858	K-9083.2	K-9264.8	K-9940.3	K-10504.5	K-11345	K-11468.3–11523.3	K-12234.5–12261.5
$T(1)-O(1)$		1.661	1.666	1.637	1.663	1.648	1.645	1.651	1.650
$T(1)-O(5)$		1.680	1.686	1.664	1.685	1.670	1.670	1.674	1.675
$T(1)-O(6)$		1.675	1.681	1.659	1.679	1.665	1.665	1.668	1.671
$T(1)-O(7)$		1.650	1.658	1.637	1.654	1.642	1.643	1.646	1.649
$<T(1)-O>$		1.667	1.673	1.649	1.670	1.656	1.656	1.660	1.661
$T(2)-O(2)$		1.634	1.631	1.625	1.633	1.630	1.630	1.633	1.627
$T(2)-O(4)$		1.605	1.601	1.601	1.609	1.604	1.604	1.606	1.602
$T(2)-O(5)$		1.648	1.648	1.648	1.647	1.647	1.650	1.648	1.649
$T(2)-O(6)$		1.663	1.660	1.665	1.660	1.663	1.665	1.663	1.664
$<T(2)-O>$		1.638	1.635	1.635	1.637	1.636	1.637	1.638	1.636
$M(1)-O(1)$	$\times 2$	2.066	2.065	2.068	2.064	2.065	2.066	2.067	2.065
$M(1)-O(2)$	$\times 2$	2.148	2.163	2.126	2.156	2.137	2.133	2.140	2.143
$M(1)-O(3)$	$\times 2$	2.115	2.112	2.110	2.115	2.109	2.111	2.110	2.112
$<M(1)-O>$		2.110	2.113	2.101	2.112	2.104	2.103	2.106	2.107
$M(2)-O(1)$	$\times 2$	2.063	2.063	2.095	2.052	2.070	2.082	2.066	2.087
$M(2)-O(2)$	$\times 2$	2.061	2.069	2.074	2.055	2.058	2.068	2.053	2.077
$M(2)-O(4)$	$\times 2$	1.968	1.970	1.982	1.958	1.963	1.970	1.959	1.982
$<M(2)-O>$		2.031	2.034	2.050	2.022	2.030	2.040	2.026	2.049
$M(3)-O(1)$	$\times 4$	2.117	2.125	2.102	2.122	2.110	2.107	2.112	2.113
$M(3)-O(3)$	$\times 2$	2.101	2.103	2.088	2.098	2.093	2.093	2.098	2.096
$<M(3)-O>$		2.112	2.118	2.097	2.114	2.104	2.102	2.108	2.107
$M(4)-O(2)$	$\times 2$	2.415	2.413	2.405	2.410	2.405	2.409	2.407	2.414
$M(4)-O(4)$	$\times 2$	2.337	2.339	2.330	2.334	2.331	2.337	2.330	2.338
$M(4)-O(5)$	$\times 2$	2.675	2.677	2.710	2.660	2.687	2.689	2.677	2.695
$M(4)-O(6)$	$\times 2$	2.543	2.548	2.542	2.546	2.536	2.542	2.537	2.552
$<M(4)-O>$		2.493	2.494	2.497	2.488	2.490	2.494	2.488	2.500
$A(2/m)-O(5)$	$\times 4$	3.045	3.051	3.020	3.048	3.027	3.031	3.032	3.037
$A(2/m)-O(6)$	$\times 4$	3.145	3.145	3.152	3.135	3.149	3.144	3.144	3.141
$A(2/m)-O(7)$	$\times 2$	2.521	2.519	2.510	2.511	2.512	2.521	2.502	2.518
$<A(2/m)-O>$		2.980	2.982	2.971	2.975	2.973	2.974	2.971	2.975
$A(m)-O(5)$	$\times 2$	3.037	3.023	2.996	3.042	3.003	3.013	3.016	3.022
$A(m)-O(5)$	$\times 2$	3.146	3.195	3.151	3.147	3.156	3.133	3.146	3.139
$A(m)-O(6)$	$\times 2$	2.779	2.744	2.762	2.771	2.761	2.799	2.768	2.787
$A(m)-O(7)$		2.515	2.566	2.533	2.504	2.539	2.523	2.513	2.515
$A(m)-O(7)$		2.640	2.615	2.619	2.630	2.614	2.619	2.611	2.625
$A(m)-O(7)$		3.224	3.189	3.181	3.233	3.200	3.244	3.217	3.237
$<A(m)-O>$		2.923	2.922	2.906	2.921	2.910	2.920	2.911	2.919
$A(2)-O(5)$	$\times 2$	2.626	2.620	2.650	2.626	2.592	2.664	2.606	2.633
$A(2)-O(6)$	$\times 2$	2.807	2.798	2.854	2.796	2.800	2.847	2.802	2.814
$A(2)-O(7)$	$\times 2$	2.576	2.578	2.553	2.567	2.571	2.564	2.559	2.570
$<A(2)-O>$		2.670	2.665	2.686	2.663	2.654	2.692	2.656	2.672
$T(1)-O(5)-T(2)$		134.62	134.6	135.4	134.1	134.90	135.0	134.61	135.09
$T(1)-O(6)-T(2)$		139.15	139.1	139.1	139.1	139.37	138.9	139.45	138.56
$T(1)-O(7)-T(1)$		140.6	140.1	140.5	140.5	140.8	140.4	140.5	139.9
$T(1)-T(2)-T(1)$		118.6	118.6	118.6	118.6	118.6	118.6	118.7	118.6
$T(2)-T(1)-T(1)$		120.3	120.3	120.4	120.3	120.3	120.3	120.3	120.4

* Standard deviations are $\leqslant 2$ in the final digit.

TABLE 4. Refined site-scattering values (e.p.f.u.) and corresponding values calculated from the unit formulae derived from EMPA for the Kola amphiboles.

	K-4967	K-6452.2	K-6600	K-6946	K-7277.2	K-7536	K-7681.2	K-8451	K-8746.2
$M(1)$	40.5	33.1	37.2	39.8	37.5	39.6	37.8	38.1	43.0
$M(2)$	35.6	29.9	33.0	31.8	33.0	35.1	33.1	33.8	36.8
$M(3)$	23.0	17.8	21.0	22.0	20.3	22.3	21.1	21.3	24.2
$\Sigma M(1,2,3)$	99.1	80.8	91.2	93.6	90.8	97.0	92.0	93.2	104.0
$\Sigma M(1,2,3)^{MP}$	97.6	81.1	90.9	92.9	90.1	96.9	91.5	93.3	103.6
$M(4)$	40.3	40.6	40.5	40.6	40.4	40.5	40.1	40.4	39.7
$M(4)^{MP}$	39.3	40.0	39.1	40.0	39.2	39.1	38.8	39.1	39.0
A	4.7	2.4	4.6	4.8	4.2	7.2	4.3	5.1	8.6
A^{MP}	4.9	2.3	4.0	5.4	3.5	7.0	3.7	5.0	8.4

	K-8858	K-9083.2	K-9264.8	K-9940.3	K-10504.5	K-11345	K-11468.3–11523.3	K-12234.5–12261.5
$M(1)$	40.2	43.7	35.5	41.2	37.9	36.5	37.2	38.5
$M(2)$	34.1	37.1	32.6	35.0	31.3	32.1	32.5	36.4
$M(3)$	22.8	24.5	19.4	23.2	21.0	23.3	20.9	21.5
$\Sigma M(1,2,3)$	97.1	105.3	87.5	99.4	90.2	88.9	90.6	96.4
$\Sigma M(1,2,3)^{MP}$	96.8	104.9	87.7	98.5	90.5	89.3	90.2	96.1
$M(4)$	40.3	40.2	40.1	40.3	40.6	40.2	40.4	40.1
$M(4)^{MP}$	39.2	39.0	39.1	38.9	38.8	39.4	39.1	38.7
A	6.8	8.6	3.8	6.9	4.7	5.9	4.8	7.3
A^{MP}	6.5	8.3	3.5	6.8	4.2	6.0	4.8	7.0

Standard deviations are $\leqslant 2$ in the final digit for SREF data.

compositional zoning and to obtain a representative composition for the whole crystal used in the collection of the diffraction data. Data reduction was done using the method of Pouchou and Pichoir (1985) and the resultant mean analysis for each grain is given in Table 5. The H_2O values were calculated in two different ways based on two models used for the site assignment of Ti, as discussed later.

Mössbauer spectroscopy

Spectra were collected on a Mössbauer milliprobe at room temperature using a point γ-ray source. Typical spectra are shown in Fig. 2. There is significant fine structure in both the upper-velocity (~2.4 mm/s) and the lower-velocity (~0.0 mm/s) envelopes, with a prominent satellite maximum to the higher-velocity side of the lower-velocity envelope (at ~0.8 mm/s). The upper-velocity envelope consists of high-velocity components of doublets due to [6]-coordinated Fe^{2+}. The satellite maximum at ~0.8 mm/s is the high-velocity component of a doublet due to [6]-coordinated-Fe^{3+}. The main part of the lower-velocity envelope consists of the low-velocity components of [6]-coordinated-Fe^{2+} doublets, together with the low-velocity component of the [6]-coordinated-Fe^{3+} doublet. The resulting isomer shifts and quadrupole-splitting values are in accord with the valences indicated above (Hawthorne, 1981, 1983*a*, 1988). The [6]-coordinated-Fe^{2+} doublets result from Fe^{2+} at the $M(1)$, $M(2)$ and $M(3)$ sites. It is apparent from the spectra in Fig. 2 that fitting three Fe^{2+} doublets to these spectra will not be straightforward as, from a least-squares perspective, the problem is extremely ill-determined. Fortunately, we are interested in the total Fe^{2+} content, not the individual Fe^{2+} site-populations (as these will be determined by site-scattering refinement). Thus, the spectra were fitted to two Fe^{2+} doublets and one Fe^{3+} doublet, and as a result, derivation of the area ratios of the peaks due to Fe^{2+} and Fe^{3+} was straightforward.

The derivation of $Fe^{3+}/(Fe^{2+}+Fe^{3+})$ values is less straightforward. The Mössbauer effect involves the recoil-free emission and absorption

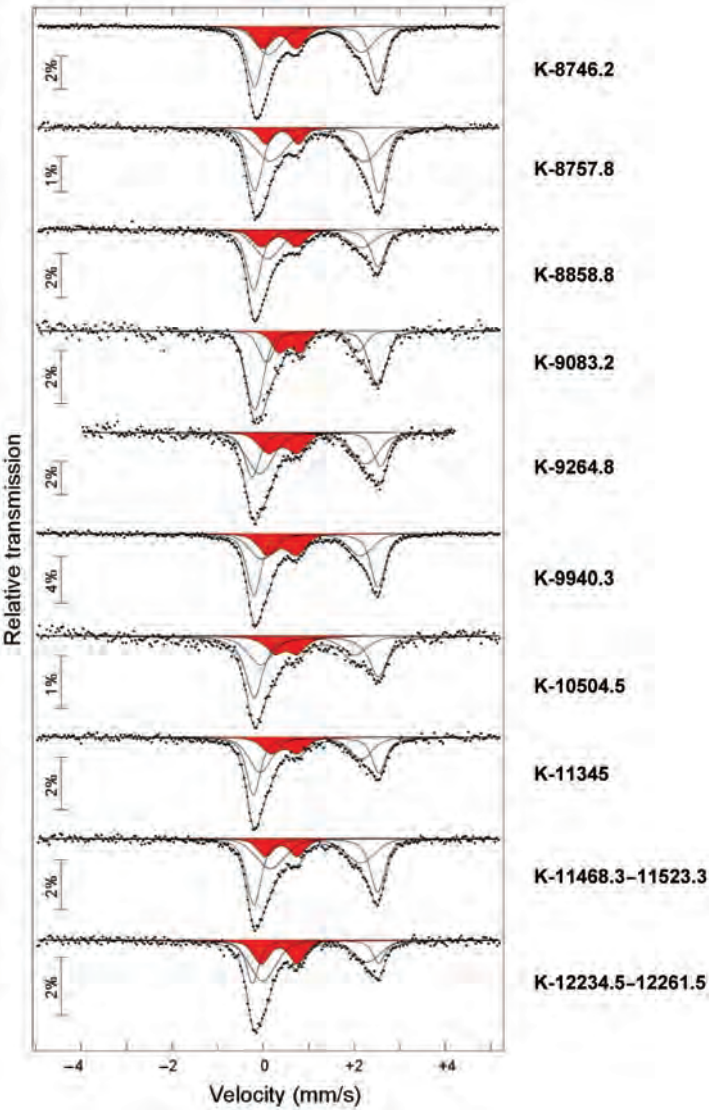

FIG. 2. Mössbauer spectra for some of the amphiboles examined here. The doublets assigned to Fe^{3+} are shown in red.

of γ-rays by a specific atomic nucleus, and the intensity of the absorption is controlled by the fraction of nuclei that are involved in this recoil-free process, the recoil-free fraction (Bancroft, 1973; Hawthorne, 1988). The nuclear energy levels are affected by the effective s-electron density at the nucleus, which in turn is affected by differential shielding from (the number of) 3d-electrons, and hence the responses for Fe^{2+} and Fe^{3+} are expected to be different. As a result, the assignment of $Fe^{3+}/(Fe^{2+}+Fe^{3+})$ values here requires knowledge of the recoil-free fractions of both Fe^{2+} and Fe^{3+} in amphibole (De Grave and Van Alboom, 1991; Eeckhout and De Grave, 2003; Dyar *et al.*, 2006). Most past studies of amphiboles have assumed that the recoil-free fractions for Fe^{2+} and Fe^{3+} are the same. However, Van Alboom and De Grave (1996) measured the recoil-free fractions of Fe^{2+} and Fe^{3+} in riebeckite and showed that the recoil-free fraction for Fe^{3+} is significantly larger than that for Fe^{2+}; Fe^{3+}:Fe^{2+} = 0.85:0.74. In the absence of

TABLE 5. Chemical composition and unit formulae* for the Kola amphiboles.

	K-4967	K-6452.2	K-6600	K-6946	K-7277.2	K-7536	K-7681.2	K-8451	K-8746.2
SiO_2	42.17	50.46	45.79	43.91	47.93	42.28	45.76	43.71	40.61
Al_2O_3	13.35	6.54	9.68	12.32	7.47	11.50	9.75	11.64	12.87
TiO_2	0.35	0.28	0.65	0.56	0.46	1.11	0.67	0.71	0.63
Cr_2O_3	0.02	0.16	0.05	0.01	0.02	0.04	0.02	0.04	0.02
Fe_2O_3	3.89	0.55	3.39	2.24	3.13	4.72	4.39	4.10	5.12
FeO	17.11	11.87	13.88	16.30	13.74	15.06	13.22	14.74	18.44
MnO	0.25	0.28	0.27	0.30	0.32	0.29	0.27	0.35	0.38
MgO	6.95	14.33	10.48	8.64	11.31	8.25	10.34	9.23	5.72
CaO	11.42	11.96	11.76	11.61	12.08	11.65	11.81	11.19	11.48
Na_2O	1.40	0.80	1.21	1.13	0.79	1.48	1.14	1.62	1.38
K_2O	0.40	0.13	0.40	0.59	0.58	0.91	0.41	0.37	1.35
F	0.00	0.02	0.04	0.03	0.08	0.04	0.04	0.04	0.05
Cl	0.00	0.01	0.01	0.03	0.02	0.02	0.02	0.03	0.03
H_2O	1.98	2.07	2.00	1.99	2.00	1.96	2.01	1.99	1.92
O=F	0.00	0.00	−0.02	−0.01	−0.03	−0.02	−0.02	−0.02	−0.02
O=Cl	0.00	0.00	0.00	0.00	0.00	0.00	0.00	0.00	0.00
Total	99.26	99.46	99.59	99.65	99.90	99.29	99.83	99.74	99.98
Si	6.398	7.303	6.795	6.581	7.067	6.418	6.771	6.534	6.249
Al	1.602	0.697	1.205	1.419	0.933	1.582	1.229	1.466	1.751
ΣT	8.000	8.000	8.000	8.000	8.000	8.000	8.000	8.000	8.000
Ti	0.040	0.030	0.073	0.063	0.051	0.127	0.075	0.080	0.073
Al	0.785	0.419	0.488	0.757	0.365	0.475	0.471	0.585	0.583
Cr	–	0.018	–	–	–	–	–	–	–
Fe^{3+}	0.444	0.060	0.379	0.253	0.347	0.539	0.489	0.461	0.593
Fe^{2+}	2.159	1.381	1.723	1.997	1.694	1.912	1.636	1.817	2.373
Mn	–	–	0.018	–	0.040	0.037	0.034	–	0.050
Mg	1. 572	3.092	2.319	1.930	2.486	1.867	2.281	2.057	1.312
ΣC	5.000	5.000	5.000	5.000	4.983	4.957	4.986	5.000	4.984
Fe^{2+}	0.012	0.056	–	0.046	–	–	–	0.026	–
Mn	0.032	0.034	0.016	0.038	–	–	–	0.044	–
Ca	1.856	1.855	1.870	1.864	1.908	1.895	1.872	1.792	1.893
Na	0.100	0.055	0.114	0.052	0.092	0.105	0.128	0.138	0.107
ΣB	2.000	2.000	2.000	2.000	2.000	2.000	2.000	2.000	2.000
Na	0.312	0.169	0.234	0.119	0.134	0.331	0.199	0.331	0.305
K	0.077	0.024	0.076	0.216	0.109	0.176	0.077	0.071	0.265
ΣA	0.389	0.193	0.310	0.335	0.243	0.507	0.276	0.402	0.570
F	0.000	0.000	0.019	0.014	0.037	0.019	0.019	0.019	0.024
OH	2.000	2.000	1.981	1.986	1.963	1.981	1.981	1.981	1.976
ΣW	2.000	2.000	2.000	2.000	2.000	2.000	2.000	2.000	2.000

* Calculated on the basis of 24 (O + OH + F) with OH + F = 2 a.p.f.u.

direct measurement of recoil-free fractions for amphiboles of the compositions examined here, magnesiohornblende-ferrotschermakite-ferropargasite-hastingsite-edenite (Table 1), we will use the Fe^{2+} and Fe^{3+} recoil-free fractions from Alboom and De Grave (1996). The resultant $Fe^{3+}/(Fe^{2+}+Fe^{3+})$ values are given in Table 6.

Calculation of unit formulae

Using the FeO_{tot} contents of the amphiboles measured by EMPA, together with the Fe^{3+}/Fe_{tot} values of Table 6, allows us to derive the Fe_2O_3 and FeO contents; these values are both included in Table 5 and were used to calculate the unit formulae of Table 5, which was initially done on

Table 5. (*Cont.*)

	K-8858	K-9083.2	K-9264.8	K-9940.3	K-10504.5	K-11345	K-11468.3–11523.3	K-12234.5–12261.5
SiO_2	42.93	40.72	47.78	41.40	45.23	45.27	44.45	43.64
Al_2O_3	11.45	12.25	7.99	12.80	11.15	9.76	11.64	9.50
TiO_2	0.93	1.28	0.46	1.00	1.00	1.04	0.89	0.77
Cr_2O_3	0.03	0.03	0.10	0.03	0.02	0.02	0.10	0.09
Fe_2O_3	4.09	4.40	3.42	4.96	3.07	3.12	2.74	5.17
FeO	15.70	19.31	12.30	15.82	13.49	12.78	13.95	14.74
MnO	0.36	0.34	0.30	0.32	0.32	0.26	0.28	0.28
MgO	8.11	5.53	12.19	7.32	10.00	11.09	10.06	9.47
CaO	11.79	11.42	12.04	11.50	11.80	12.13	11.53	11.50
Na_2O	1.26	1.49	0.95	1.56	1.09	1.06	1.38	1.48
K_2O	0.95	1.25	0.45	0.85	0.62	0.96	0.50	1.03
F	0.05	0.04	0.03	0.08	0.04	0.03	0.08	0.02
Cl	0.04	0.04	0.02	0.02	0.02	0.03	0.04	0.02
H_2O	1.96	1.93	2.03	1.93	2.01	2.01	1.98	1.99
O=F	−0.02	−0.02	−0.01	−0.03	−0.02	−0.01	−0.03	0.00
O=Cl	0.00	0.00	0.00	0.00	0.00	0.00	0.00	0.00
Total	99.63	100.01	100.05	99.56	99.84	99.55	99.59	99.70
Si	6.492	6.279	6.992	6.293	6.682	6.719	6.598	6.592
Al	1.508	1.721	1.008	1.707	1.312	1.281	1.402	1.408
ΣT	8.000	8.000	8.000	8.000	8.000	8.000	8.000	8.000
Ti	0.106	0.148	0.051	0.114	0.111	0.116	0.099	0.087
Al	0.533	0.505	0.370	0.586	0.623	0.426	0.634	0.283
Cr	–	–	0.012	–	–	–	0.012	0.011
Fe^{3+}	0.465	0.511	0.377	0.567	0.341	0.348	0.306	0.588
Fe^{2+}	1.985	2.490	1.505	2.011	1.667	1.586	1.723	1.862
Mn	0.046	0.044	0.026	0.041	0.040	0.033	–	0.037
Mg	1.828	1.271	2.659	1.659	2.202	2.454	2.226	2.132
ΣC	4.963	4.969	5.000	4.978	4.984	4.963	5.000	5.000
Fe^{2+}	–	–	–	–	–	–	0.009	–
Mn	–	–	0.011	–	–	–	0.035	–
Ca	1.910	1.887	1.888	1.873	1.868	1.929	1.834	1.861
Na	0.090	0.113	0.101	0.127	0.132	0.071	0.122	0.139
ΣB	2.000	2.000	2.000	2.000	2.000	2.000	2.000	2.000
Na	0.279	0.333	0.169	0.333	0.180	0.234	0.275	0.294
K	0.183	0.246	0.084	0.165	0.117	0.182	0.095	0.198
ΣA	0.462	0.579	0.253	0.498	0.297	0.416	0.370	0.492
F	0.024	0.020	0.014	0.038	0.019	0.014	0.038	0.000
OH	1.976	1.980	1.986	1.962	1.981	1.986	1.962	2.000
ΣW	2.000	2.000	2.000	2.000	2.000	2.000	2.000	2.000

the basis of 24 (O, OH, F) assuming OH + F = 2.0 a.p.f.u.

The effect of Ti^{4+}

There is another issue which affects the calculation of the Fe^{3+} content of the amphibole, and that is the role assigned to Ti. It is now established that Ti is in the tetravalent state in amphiboles (Oberti *et al.*, 1992 and discussion therein). Furthermore, except for the special case of richteritic amphiboles in which Ti^{4+} can occupy the *T*(2) site, Ti^{4+} is octahedrally coordinated in amphiboles and can be assigned as a C-group cation

TABLE 6. $Fe^{3+}/Fe_{tot.}$ ratios obtained by Milli-Mössbauer spectroscopy, FeO values obtained by EMPA and Fe_2O_3 and FeO calculated values.

Sample	$Fe^{3+}/Fe_{tot.}$	FeO (wt.%)$_{EMPA}$	$FeO_{calc.}$	$Fe_2O_{3\ calc.}$
K-4967	0.13	20.61	17.52	3.44
K-6452.2	0.04	12.36	11.87	0.55
K-6600	0.14	16.93	14.22	3.01
K-6946	0.09	18.31	16.30	2.24
K-7277.2	0.13	16.56	14.08	2.76
K-7536	0.17	19.31	15.64	4.08
K-7681.2	0.18	17.17	13.74	3.82
K-8451	0.16	18.43	15.11	3.69
K-8746.2	0.16	23.05	18.90	4.61
K-8858	0.15	19.38	16.09	3.66
K-9083.2	0.13	23.27	19.78	3.88
K-9264.8	0.16	15.37	12.60	3.07
K-9940.3	0.17	20.28	16.43	4.28
K-10504.5	0.13	16.25	13.81	2.71
K-11345	0.14	15.59	13.10	2.77
K-11468.3–11523.3	0.12	16.41	14.28	2.37
K-12234.5–12261.5	0.19	19.39	15.32	4.53

(Hawthorne, 1983*b*,*c*). Oberti *et al.* (1992) showed that in (Fe-free) richterites, $^{[6]}Ti^{4+}$ occurs at the *M*(1) site, and proposed that Ti^{4+} can enter the amphibole structure via the substitution:

$$^{M(1)}Ti^{4+} + 2^{O(3)}O^{2-} \rightleftharpoons {}^{M(1)}Mg + 2^{O(3)}(OH) \qquad (1)$$

This substitution was also observed by Hawthorne *et al.* (1998) on a series of sodic-calcic and sodic amphiboles.

It has been assumed that when Ti^{4+} is present in small amounts, it occupies the *M*(2) site; however, there is no direct experimental evidence for this. The data of Hawthorne *et al.* (1998) suggest that this is the case, but the results of Oberti *et al.* (1992) disagree. The latter are probably more reliable as they are based on site populations involving small amounts of Ti^{4+} in the absence of significant Fe (i.e. the site scattering is particularly sensitive to the behaviour of Ti in this particular case). The results of Hawthorne *et al.* (1998) indicate that mechanism 1 is adhered to with great precision, but with a small (<0.11 Ti a.p.f.u.) excess of Ti^{4+} over the amount of H deficiency, which can be interpreted as Ti^{4+} occupying the *M*(2) site (a result that is not possible to confirm directly by site-scattering refinement in these particular amphiboles due to the presence of significant C-group Fe^{2+} and Fe^{3+}). Moreover, this result depends on standardization of H analysis by SIMS being correct, not to a relative amount of 0.20 H a.p.f.u., but to an absolute amount of the same magnitude, a very difficult endeavour to say the least. So, the evidence is somewhat ambiguous as to where Ti occurs in calcic amphiboles.

Mechanism 1 will have significant stereochemical effects, particularly with regard to the mean bond lengths of the *M* sites involved in this issue: *M*(1) and *M*(2). Octahedrally coordinated Ti^{4+} has a radius of 0.605 Å, whereas $^{[6]}Fe^{2+}$ and $^{[6]}Fe^{3+}$ have radii of 0.78 and 0.645 Å (Shannon, 1976). Hence whether Ti or Fe is assigned as the heavy-scatterer at a site makes a significant difference to the mean cation radius at that site. Moreover, the radius of [3]-coordinated (OH), 1.34 Å, is somewhat less than the radius of [3]-coordinated O^{2-}, 1.36 Å, a factor that will affect the calculated mean bond lengths at the *M* sites coordinating the O(3) anion. Thus the Fe^{3+} content of these amphiboles will be calculated for two different models of the behaviour of Ti^{4+}: (1) all Ti^{4+} assigned to *M*(1) and (OH) + F = 2.0 − $2Ti^{4+}$ a.p.f.u., and (2) all Ti^{4+} assigned to *M*(2) and O(3) = (OH) + F = 2.0 a.p.f.u.

Derivation of Fe^{3+} content from the refined crystal structure

This may be done using the following procedure:

(1) The unit formula is calculated with Fe^{3+} = 0.0 a.p.f.u., and the site populations are assigned (see later discussion); (2) it is well established

that, in the absence of O^{2-} at O(3), all Fe^{3+} is ordered at *M*(2); (3) there is a very well-developed linear correlation between mean bond length and aggregate constituent-cation radius for the *M*(2) site (Hawthorne, 1981, 1983*a*); the latest relation is given by Hawthorne and Oberti (2007): $\langle M(2)-O\rangle = 1.476 + 0.845 \langle r^{M(2)}\rangle$ Å; (4) as the radii of Fe^{2+} and Fe^{3+} are significantly different ($r^{Fe^{2+}} = 0.645$, $r^{Fe^{3+}} = 0.78$ Å; Shannon, 1976), we may use the relation between mean bond length and aggregate constituent-cation radius for the *M*(2) site to calculate an initial estimate of the amounts of Fe^{3+} and Fe^{2+} at *M*(2) (and hence in the amphibole); (5) these values of Fe^{3+} and Fe^{2+} are then used to calculate the Fe_2O_3 and FeO that are used to recalculate the unit formula; this unit formula is used to assign site populations; (6) steps (4) to (6) are iterated until convergence.

The Fe^{3+} contents resulting from this process, calculated with (1) Ti at the *M*(1) site; and (2) Ti at the *M*(2) site, are compared with the Mössbauer-determined Fe^{3+} contents in Fig. 5.

Site populations

Normally, site populations are assigned on the basis of (1) the refined site-scattering values (Table 4); (2) the unit formulae derived from the chemical compositions determined by EMPA (Table 5); (3) the observed bond lengths and regression equations (e.g. Hawthorne, 1983*a*,*b*) relating mean bond length to the aggregate mean radius of the constituent cations (and anions if the O(3) site is involved); (4) the constraint that all sites except *A* be fully occupied; (5) the constraint of electroneutrality. An important issue is the consistency of the refined site-scattering values with the unit formulae derived from EMPA. We may examine the issue by comparing the values derived by each method for the *A*-, *B*- and *C*-group cations. As is apparent from Fig. 3, the agreement is extremely close, emphasizing the compatibility of the EMPA and site-scattering refinement data.

The T sites

The unit formulae of Table 5 indicate that there is significant (0.697–1.751 a.p.f.u.) [4]-coordinated Al in these amphiboles. The stereochemical details of the incorporation of [4]-coordinated Al into the double-chain element of the *C*2/*m* amphibole structure have been examined by many investigators (Papike *et al.*, 1969; Hawthorne and Grundy, 1973*a*,*b*, 1977; Robinson *et al.*, 1973; Bocchio *et al.*, 1978; Hawthorne, 1981, 1983*a*,*b*; Oberti *et al.*, 1995*b*). The results of these studies are broadly in agreement: in amphiboles with considerable [4]-coordinated Al (i.e. <~0.50 a.p.f.u.), Al is strongly ordered at the *T*(1) site (Oberti *et al.*, 2007). In general, significant Al does not occur at *T*(2) until [4]-coordinated Al is >2.0 a.p.f.u., except where significant Ca occurs at the *A*(2) site (Hawthorne *et al.*, 1995), in which case Al at *T*(1) is >2.0 a.p.f.u. (and Al–O(7)–Al linkages occur, locally associated with Ca at the *A*(2) site). However, in high-temperature amphiboles (Oberti *et al.*, 1995*b*), Al can occur at *T*(2) where [4]-coordinated Al <2.00 a.p.f.u.

Hawthorne and Oberti (2007) examined the behaviour of ~150 amphiboles taken from the literature and presented very precise relations between [4]-coordinated Al and the grand mean *T*–O distance in amphibole, and also curves for assigning Al to the *T*(1) and *T*(2) sites based on the $\langle T(1)-O\rangle$ and $\langle T(2)-O\rangle$ distances. Tetrahedrally coordinated Al was assigned to the *T*(1) and *T*(2) sites in the following manner: (1) preliminary values were assigned from the observed $\langle T(1)-O\rangle$ and $\langle T(2)-O\rangle$ distances (Table 3); (2) the individual site populations were adjusted such that the sum of the site populations lay halfway between the observed (unit formulae) and predicted (sum of the *T*(1) and *T*(2) site-populations) total tetrahedrally coordinated Al content (i.e. assuming similar random error in both values). The resulting values are given in Table 7.

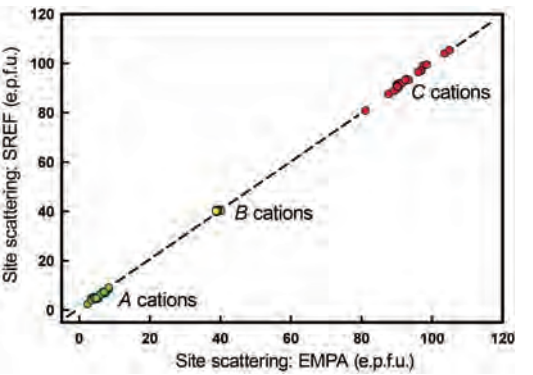

FIG. 3. Comparison of the effective site-scattering (in e.p.f.u.: electrons per formula unit) determined by site-scattering refinement (SREF) and EMPA for the *A*-, *B*- and *C*-group cations in Kola amphiboles; the line is the 1:1 relation.

The M(1,2,3) sites

The unit formulae (Table 5) indicate that these sites are occupied by Mg, Fe^{2+}, Mn^{2+}, Al, Fe^{3+}, Cr^{3+} and Ti^{4+}, and Fig. 3 indicates that the *C*-group scattering is in accord with the unit formulae of Table 5. As the refined site-scattering values provide information on the occupancy of only two species per site, we need to use other information to derive complete site populations. Based on extensive previous work on amphiboles, Fe^{3+} and Cr^{3+} were assigned to the *M*(2) site. Any *C*-group cations >5.00 a.p.f.u. were assigned as Mn^{2+} (and Fe^{2+} where Mn^{2+} is insufficient) at the *M*(4) site. Any remaining Mn^{2+} was combined with Fe^{2+} as their X-ray-scattering is very similar. Octahedrally-coordinated Al constitutes more of a problem. In most crystallographic studies, $^{[6]}$Al has been assigned to the *M*(2) site. However, Oberti *et al.* (1995*b*) showed that in calcic amphiboles of pargasitic composition, $^{[6]}$Al is partly ordered over the *M*(2) and *M*(3) sites, and the degree of this disorder is a sensitive function of the Mg content of the amphibole, with considerable disorder in Mg-rich crystals. Comparison of the amphibole compositions refined here with those of Oberti *et al.* (1995*b*), suggests that the crystals of the present study will not show extensive $^{[6]}$Al disorder, and hence we assigned all $^{[6]}$Al to the *M*(2) site. At this stage, we can assign Mg and Fe to the *M*(1), *M*(2) and *M*(3) sites on the basis of the refined site-scattering values (Table 4), with all Fe^{3+} assigned to *M*(2). The resultant populations for these sites are given in Table 7.

The M(4) site

The chemical compositions shown in Table 5 indicate that the *M*(4) site is dominated by Ca in

TABLE 7. Site populations (a.p.f.u.) for the Kola amphiboles.

		K-4967	K-6452.2	K-6600	K-6946	K-7277.2	K-7536	K-7681.2	K-8451	K-8746.2
T(1)	Al	1.48	0.63	1.08	1.26	0.85	1.43	1.11	1.32	1.64
	Si	2.52	3.37	2.92	2.74	3.15	2.57	2.89	2.68	2.36
T(2)	Al	0.17	0.13	0.19	0.20	0.14	0.22	0.24	0.20	0.19
	Si	3.83	3.87	3.81	3.80	3.86	3.78	3.76	3.80	3.81
M(1)	Mg	0.851	1.340	1.047	0.901	1.056	0.886	1.034	0.993	0.653
	Fe	1.149	0.660	0.953	1.099	0.944	1.114	0.966	1.007	1.347
M(2)	Ti	0.040	0.030	0.073	0.063	0.051	0.128	0.075	0.080	0.073
	Fe^{3+}	0.444	0.060	0.379	0.253	0.348	0.544	0.490	0.461	0.595
	Cr^{3+}	–	0.018	–	–	–	–	–	–	–
	Al	0.785	0.419	0.488	0.757	0.366	0.479	0.472	0.585	0.585
	Fe^{2+}	0.300	0.294	0.177	0.205	0.232	0.123	0.072	0.140	0.226
	Mg	0.431	1.179	0.883	0.722	1.003	0.726	0.891	0.734	0.521
M(3)	Mg	0.244	0.576	0.379	0.306	0.424	0.262	0.358	0.336	0.130
	Fe^{2+}	0.756	0.424	0.603	0.694	0.536	0.701	0.608	0.664	0.820
	Mn	–	–	0.018	–	0.040	0.037	0.034	–	0.050
M(4)	Fe^{2+}	0.012	0.056	–	0.046	–	–	–	0.026	–
	Mn	0.032	0.034	0.016	0.038	–	–	–	0.044	–
	Ca	1.856	1.855	1.870	1.864	1.908	1.895	1.872	1.792	1.893
	Na	0.100	0.055	0.114	0.052	0.092	0.105	0.128	0.138	0.107
A	Na	0.312	0.169	0.234	0.119	0.134	0.331	0.199	0.331	0.305
	K	0.077	0.024	0.079	0.216	0.109	0.176	0.077	0.071	0.265
	Σ	0.389	0.193	0.313	0.335	0.243	0.507	0.276	0.402	0.570
O(3)	OH	2.000	2.000	1.981	1.986	1.963	1.981	1.981	1.981	1.976
	F	0.000	0.000	0.019	0.014	0.037	0.019	0.019	0.019	0.024
	Σ	2.000	2.000	2.000	2.000	2.000	2.000	2.000	2.000	2.000

these crystals, with the balance made up of Na. The resultant site populations are in close accord with the refined site-scattering values at this site (Fig. 3).

The A site

The *A* site is partly occupied by Na and K in these amphiboles. The refined site-scattering values are in accord with the chemical compositions given in Table 5 (Fig. 3). In the monoclinic amphiboles, there is significant positional disorder of Na and K within the *A* cavity. Potassium occupies the *A*(*m*) site, and Na can occupy the *A*(*m*) and *A*(2) sites (Papike *et al.*, 1969; Hawthorne and Grundy, 1972, 1973*a*,*b*; Hawthorne, 1981, 1983*b*,*c*; Hawthorne *et al.*, 1996). This issue is examined in Fig. 4 for the structures refined in this study. This shows typical difference-Fourier maps calculated with the *A*-site cations removed from the refinement model. The range of behaviour is small compared with that exhibited in amphiboles (Hawthorne *et al.*, 1996). Figure 4*a* shows the majority of the electron density at the *A*(2) site, with a smaller amount at *A*(*m*), whereas Fig. 4*c* shows a greater amount of density at the *A*(*m*) site with somewhat less at the *A*(2) site; Fig. 4*b* shows approximately the same density at the *A*(*m*) and *A*(2) sites. Inspection of Table 5 shows that all crystals shown in Fig. 4 have similar amounts of *A*-site Na (0.275–0.333 a.p.f.u.), whereas they have a greater range in K content (0.095–0.246 a.p.f.u.). Previous work (summarized by Hawthorne and Oberti, 2007; Hawthorne and Della Ventura, 2007) has shown that K occurs only at the *A*(*m*) site, in accord with the greater density at that site in crystal K-9083.2

Table 7. (*Cont.*)

		K-8858	K-9083.2	K-9264.8	K-9940.3	K-10504.5	K-11345	K-11468.3–11523.3	K-12234.5–12261.5
T(1)	Al	1.40	1.64	0.89	1.55	1.14	1.11	1.23	1.27
	Si	2.60	2.36	3.11	2.45	2.86	2.89	2.77	2.73
T(2)	Al	0.24	0.17	0.17	0.22	0.20	0.22	0.25	0.20
	Si	3.76	3.83	3.83	3.78	3.80	3.78	3.75	3.80
M(1)	Mg	0.853	0.603	1.179	0.801	1.007	1.097	1.057	0.964
	Fe	1.147	1.397	0.821	1.199	0.993	0.903	0.943	1.036
M(2)	Ti	0.107	0.149	0.051	0.115	0.111	0.117	0.099	0.087
	Fe^{3+}	0.468	0.514	0.377	0.570	0.342	0.351	0.306	0.588
	Cr^{3+}	–	–	0.012	–	–	–	0.012	0.011
	Al	0.537	0.508	0.370	0.588	0.625	0.429	0.634	0.283
	Fe^{2+}	0.139	0.279	0.164	0.092	0.056	0.113	0.175	0.205
	Mg	0.749	0.550	1.026	0.635	0.866	0.990	0.774	0.826
M(3)	Mg	0.230	0.114	0.469	0.217	0.354	0.395	0.364	0.319
	Fe^{2+}	0.724	0.842	0.505	0.742	0.606	0.572	0.636	0.644
	Mn	0.046	0.044	0.026	0.041	0.040	0.033	–	0.037
M(4)	Fe^{2+}	–	–	–	–	–	–	0.009	–
	Mn	–	–	0.011	–	–	–	0.035	–
	Ca	1.910	1.887	1.888	1.873	1.868	1.929	1.834	1.861
	Na	0.090	0.113	0.101	0.127	0.132	0.071	0.122	0.139
A	Na	0.279	0.333	0.169	0.333	0.180	0.234	0.275	0.294
	K	0.183	0.246	0.084	0.165	0.117	0.182	0.095	0.198
	Σ	0.462	0.579	0.253	0.498	0.297	0.416	0.370	0.492
O(3)	OH	1.976	1.980	1.986	1.962	1.981	1.986	1.962	2.000
	F	0.024	0.020	0.014	0.038	0.019	0.014	0.038	–
	Σ	2.000	2.000	2.000	2.000	2.000	2.000	2.000	2.000

(Fig. 4*c*) (K = 0.246 a.p.f.u.) than in the other two crystals shown in Fig. 6 (0.077–0.095 K a.p.f.u.). Examination of Fig. 4 (and the other difference-Fourier maps) shows that most (if not all) of the *A*-site Na occurs at the *A*(2) site (as in K-4967, Fig. 4*a*).

Hawthorne *et al.* (1996) showed that the occupancies of the *A*(*m*) and *A*(2) sites by Na in *C*2/*m* amphiboles are dictated by short-range bond valence requirements. The authors listed an order of preference for the patterns of short-range order: $^{M(4)}$Na–$^{O(3)}$F–$^{A(m)}$Na > $^{M(4)}$Ca–$^{O(3)}$OH–$^{A(2)}$Na > $^{M(4)}$Ca–$^{O(3)}$OH–$^{A(m)}$Na > $^{M(4)}$Ca–$^{O(3)}$F–$^{A(m)}$Na > $^{M(4)}$Ca–$^{O(3)}$F–$^{A(2)}$Na. The F contents of the amphiboles examined are negligible (Table 6) and we can discount significant amounts of the arrangements involving $^{O(3)}$F. Thus, the occupancies of *A*(2) and *A*(*m*) will be controlled by the preference $^{M(4)}$Ca–$^{O(3)}$OH–$^{A(2)}$Na > $^{M(4)}$Ca–$^{O(3)}$OH–$^{A(m)}$Na. As all constituents of these two arrangements are the same (apart from the *A*-site Na itself), we predict from the compositions of these amphiboles that *A*-site Na will occur at *A*(2) rather than *A*(*m*); inspection of Fig. 4 shows that this is the case.

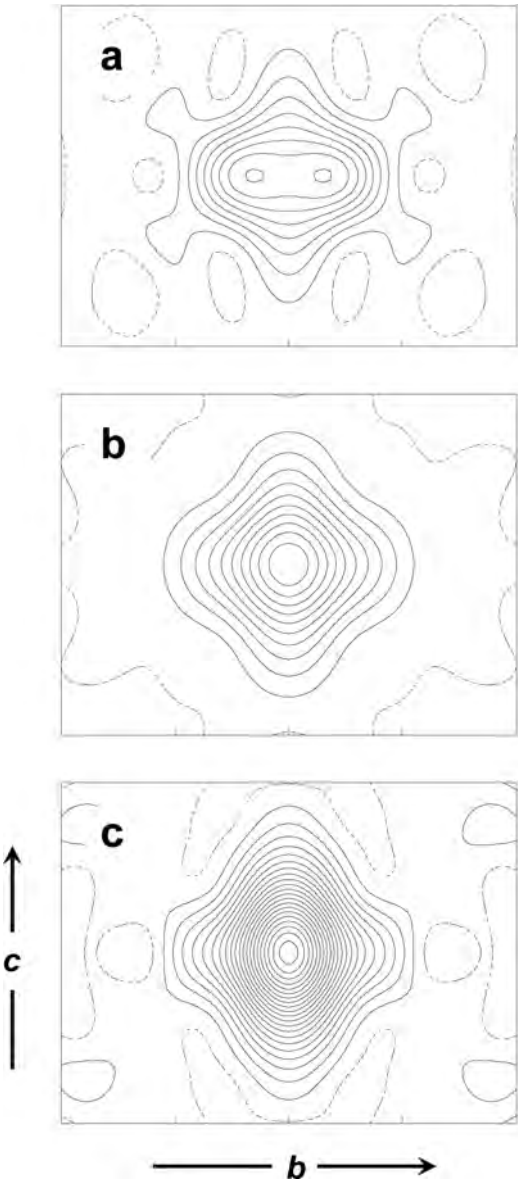

FIG. 4. Selected *A*-site difference-Fourier sections parallel to $\bar{2}01$, showing the electron density in the *A* cavity for three of the Kola amphiboles; (a) K-4967; (b) K-11468.3–11523.3; (c) K-9083.2. The contour interval is 0.5 *e*/Å^3, and the broken line is the zero contour.

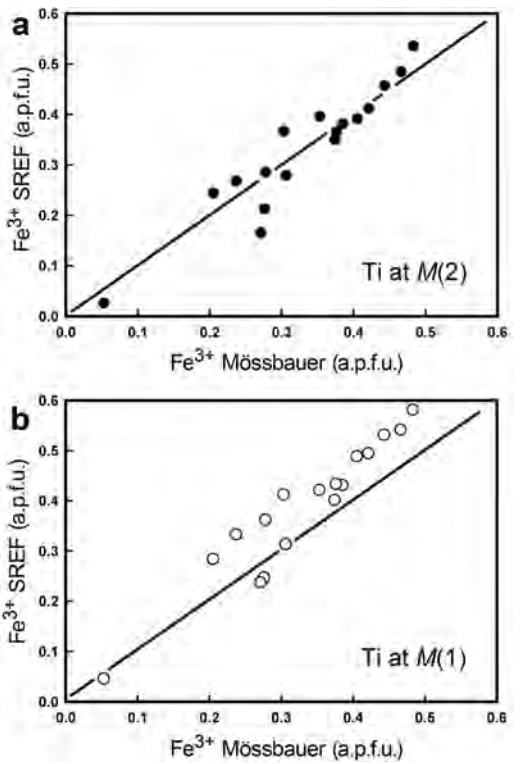

FIG. 5. Variation in Fe^{3+} determined by SREF assuming all Ti^{4+} is ordered at (*a*) *M*(2) and (*b*) *M*(1) as a function of Fe^{3+} determined by Mössbauer spectroscopy.

Fe^{3+} in amphiboles by SREF and Mössbauer spectroscopy

The key issue in this work involves assessment of the accuracy of SREF determination of Fe^{3+} in amphiboles; this point is examined in detail in Fig. 5. Figure 5*a* shows a comparison of Fe^{3+} calculated assuming Ti^{4+} is fully ordered at *M*(2) and the amount of Fe^{3+} observed by combined Mössbauer spectroscopy and EMPA. The data scatter about the 1:1 line, indicating excellent agreement between the two techniques. Figure 5*b* shows a similar comparison involving Fe^{3+} calculated assuming Ti^{4+} is fully-ordered at *M*(1); apart from a few points, the data scatter above the 1:1 line. Comparison of Figs 5*a* and 5*b* indicates that, in most cases, Ti^{4+} is ordered at *M*(2). Hence, we can conclude that SREF, in combination with EMPA, does give accurate values of Fe^{3+} in amphiboles.

Acknowledgements

YU was supported by a Manitoba Graduate Fellowship. FCH was supported by a Canada Research Chair in Crystallography and Mineralogy, and by Research Tools and Equipment, Discovery and Major Facilities Access grants from the Natural Sciences and Engineering Research Council of Canada, and by Innovation Grants from the Canada Foundation for Innovation. VIK and KVB were supported by the Russian Foundation for Basic Research. This work was completed as part of a Special Research Agreement between the Institute of Geology of Ore Deposits, Petrography, Mineralogy and Geochemistry, Russian Academy of Sciences, and the University of Manitoba.

References

Bancroft, G.M. (1973) *Mössbauer Spectroscopy. An Introduction for Inorganic Chemists and Geochemists.* McGraw-Hill, New York.

Bocchio, R., Ungaretti, L. and Rossi, G. (1978) Crystal chemical study of eclogitic amphiboles from Alpe Arami, Lepontine Alps, Southern Switzerland. *Rendiconti della Societa Italiana di Mineralogia e Petrologia*, **34**, 453–470.

De Grave, E. and Van Alboom, A. (1991) Evaluation of ferrous and ferric Mossbauer fractions. *Physics and Chemistry of Minerals*, **18**, 337–342.

Delaney, J.S., Bajt, S., Sutton, S.R. and Dyar, M.D. (1996) In situ microanalysis of $Fe^{3+}/\Sigma Fe$ in amphibole by X-ray absorption near edge structure (XANES) spectroscopy. Pp. 165–171 in: *Mineral Spectroscopy: A Tribute to Roger G. Burns.* (M.D. Dyar, C. McCammon and M.W. Schaefer, editors). Geochemical Society Special Publication, **5**.

Dyar, M.D., McGuire, A.V. and Mackwell, S.J. (1992) Fe^{3+}/H^{+} and D/H in kaersutites: Misleading indicators of mantle source fugacities. *Geology*, **20**, 565–568.

Dyar, M.D., Mackwell, S.J., McGuire, A.V., Cross, L.R. and Robertson, J.D. (1993) Crystal chemistry of Fe^{3+} and H^{+} in mantle kaersutite: Implications for mantle metasomatism. *American Mineralogist*, **78**, 968–979.

Dyar, M.D., Gunter, M.E., Delaney, J.S., Lanzarotti, A. and Sutton, S.R. (2002) Systematics in the structure and XANES spectra of pyroxenes, amphiboles, and micas as derived from oriented single crystals. *The Canadian Mineralogist*, **40**, 1375–1393.

Dyar, M.D., Agresti, D.G., Schaefer, M.W., Grant, C.A. and Sklute, E.C. (2006) Mössbauer Spectroscopy of Earth and Planetary Materials. *Annual Review of Earth and Planetary Science*, **34**, 83–125.

Eeckhout, S.G. and De Grave, E. (2003) Evaluation of ferrous and ferric Mössbauer fractions. Part II. *Physics and Chemistry of Minerals*, **30**, 142–146.

Enders, M., Speer, D., Maresch, W.V. and McCammon, C.A. (2000) Ferric/ferrous iron ratios in sodic amphiboles: Mössbauer analysis, stoichiometry-based model calculations and the high-resolution microanalytical flank method. *Contributions to Mineralogy and Petrology*, **140**, 135–147.

Garvie, L.A.J. and Buseck, P.R. (1998) Ratios of ferrous to ferric iron from nanometer-sized areas in minerals. *Nature*, **396**, 667–670.

Garvie, L.A.J., Zega, T.J., Rez, P. and Buseck, P.R. (2004) Nanometer-scale measurements of $Fe^{3+}/\Sigma Fe$ by electron energy-loss spectroscopy: A cautionary note. *American Mineralogist*, **89**, 1610–1616.

Hawthorne, F.C. (1981) Crystal chemistry of the amphiboles. *Reviews in Mineralogy*, **9A**, 1–102.

Hawthorne, F.C. (1983*a*) Quantitative characterization of site occupancies in minerals. *American Mineralogist*, **68**, 287–306.

Hawthorne, F.C. (1983*b*) The crystal chemistry of the amphiboles. *The Canadian Mineralogist*, **21**, 353–480.

Hawthorne, F.C. (1983*c*) Characterization of the average structure of natural and synthetic amphiboles. *Periodica Mineral Roma*, **52**, 543–581.

Hawthorne, F.C. (1988) Mössbauer spectroscopy. *Reviews in Mineralogy*, **18**, 255–340.

Hawthorne, F.C. and Della Ventura, G. (2007) Short-range order in amphiboles. Pp. 173–223 in: *Amphiboles: Crystal Chemistry, Occurrence, and Health Issues* (F.C. Hawthorne, R. Oberti, G. Della

Ventura and A. Mottana, editors). Reviews in Mineralogy and Geochemistry **67**, Mineralogical Society of America, Washington, D.C.

Hawthorne, F.C. and Grundy, H.D. (1972) Positional disorder in the *A*-site of clino-amphiboles. *Nature*, **235**, 72.

Hawthorne, F.C. and Grundy, H.D. (1973*a*) The crystal chemistry of the amphiboles. I. Refinement of the crystal structure of ferrotschermakite. *Mineralogical Magazine*, **39**, 36–48.

Hawthorne, F.C. and Grundy, H.D. (1973*b*) The crystal chemistry of the amphiboles. II. Refinement of the crystal structure of oxykaersutite. *Mineralogical Magazine*, **39**, 390–400.

Hawthorne, F.C. and Grundy, H.D. (1977) The crystal chemistry of the amphiboles. III. Refinement of the crystal structure of a sub-silicic hastingsite. *Mineralogical Magazine*, **41**, 43–50.

Hawthorne, F.C. and Oberti, R. (2007) Amphiboles: crystal chemistry. Pp. 1–54 in: *Amphiboles: Crystal Chemistry, Occurrence, and Health Issues* (F.C. Hawthorne, R. Oberti, G. Della Ventura and A. Mottana, editors). Reviews in Mineralogy and Geochemistry **67**, Mineralogical Society of America, Chantilly, VA, and the Geochemical Society, Washington, D.C.

Hawthorne, F.C., Ungaretti, L., Oberti, R., Bottazzi, P. and Czamanske, G.K. (1993) Li: An important component in igneous alkali amphiboles. *American Mineralogist*, **78**, 733–745.

Hawthorne, F.C., Ungaretti, L., Oberti, R., Cannillo, E. and Smelik, E.A. (1994) The mechanism of $^{[6]}$Li incorporation in amphiboles. *American Mineralogist*, **79**, 443–451.

Hawthorne, F.C., Oberti, R., Cannillo, E., Sardone, N., Zanetti, A., Grice, J.D. and Ashley, P.M. (1995) A new anhydrous amphibole from the Hoskins mine, Grenfell, New South Wales, Australia: Description and crystal structure of ungarettiite, $NaNa_2(Mn_2^{2+}Mn_3^{3+})Si_8O_{22}O_2$. *American Mineralogist*, **80**, 165–172.

Hawthorne, F.C., Oberti, R. and Sardone, N. (1996) Sodium at the *A* site in clinoamphiboles: the effects of composition on patterns of order. *The Canadian Mineralogist*, **34**, 577–593.

Hawthorne, F.C., Oberti, R., Zanetti, A. and Czamanske, G.K. (1998) The role of Ti in hydrogen-deficient amphiboles: Sodic-calcic and sodic amphiboles from Coyote Peak, California. *The Canadian Mineralogist*, **36**, 1253–1265.

Höfer, H.E., Brey, G.P., Schulz-Dobrick, B. and Oberhänsli, R. (1994) The determination of the iron oxidation state by the electron microprobe. *European Journal of Mineralogy*, **6**, 407–418.

Isanina, E.V., Verba, M.L., Ivanova, N.M., Kazansky, V.I. and Sharov, N.V. (2000) Deep structure and seismogeological boundaries of the Pechenga District of the Baltic Shield and the adjacent part of the Barents Sea shelf plate. *Geology of Ore Deposits*, **42**, 429–439.

Kazansky, V.I. (1992) Deep structure and metallogeny of Early Proterozoic mobile belts in the light of superdeep drilling in Russia. *Precambrian Research*, **58**, 289–303.

Kazansky, V.I. (1997) New findings of the Kola Superdeep Borehole. *Journal of Journals*, **1997**, 79–86.

Kazansky, V.I., Isanina, E.V., Lobanov, K.V., Predovsky, A.A. and Sharov, N.V. (2002) Geological-geophysical setting, seismological boundaries and metallogeny of the Pechenga ore district. *Geology of Ore Deposits*, **44**, 242–251.

King, P.L., Hervig, R.L., Holloway, J.R., Vennemann, T.W. and Righter, K. (1999) Oxy-substitution and dehydrogenation in mantle-derived amphibole megacrysts. *Geochimica Cosmochimica Acta*, **62**, 3635–3651.

Lobanov, K.V., Kazansky, V.I., Kuznetsov, A.V., Zharikov, A.V., Nikitin, A.N., Ivankina, T.I. and Zamyatina, N.V. (2002) Correlation of Archean rocks from the Kola Superdeep Borehole and their analogues from the surface: Evidence from structural-petrological, petrophysical, and neutron diffraction data. *Petrology*, **10**, 23–38.

Martin, R.F. (2007) Amphiboles in the igneous environment. Pp. 323–358 in: *Amphiboles: Crystal Chemistry, Occurrence, and Health Issues* (F.C. Hawthorne, R. Oberti, G. Della Ventura and A. Mottana, editors). Reviews in Mineralogy and Geochemistry **67**, Mineralogical Society of America, Chantilly, VA, and the Geochemical Society, Washington, D.C.

McCammon, C.A. (1994) A Mössbauer milliprobe: Practical considerations. *Hyperfine Interactions*, **92**, 1235–1239.

Nikitina, L.P., Ovchinnikov, N.O., Yakovleva, A.K., Chernova, O.G. and Goilo, E.A. (2002) Defect crystal structures of micas in ultramafites and mafites from the Kola superdeep borehole. *Proceedings of the Russian Mineralogical Society*, **131**, 23–44 (in Russian).

Oberti, R., Ungaretti, L., Cannillo, E. and Hawthorne, F.C. (1992) The behaviour of Ti in amphiboles. I. Four- and six-coordinate Ti in richterite. *European Journal of Mineralogy*, **3**, 425–439.

Oberti, R., Hawthorne, F.C., Ungaretti, L. and Cannillo, E. (1995*a*) $^{[6]}$Al disorder in amphiboles from mantle peridotites. *The Canadian Mineralogist*, **33**, 867–878.

Oberti, R., Ungaretti, L., Cannillo, E., Hawthorne, F.C. and Memmi, I. (1995*b*) Temperature-dependent Al order-disorder in the tetrahedral double-chain of

*C*2/*m* amphiboles. *European Journal of Mineralogy*, **7**, 1049–1063.

Oberti, R., Hawthorne, F.C., Cannillo, E. and Camara, F. (2007) Long-range order in amphiboles. Pp. 125–171 in: *Amphiboles: Crystal Chemistry, Occurrence, and Health Issues* (F.C. Hawthorne, R. Oberti, G. Della Ventura and A. Mottana, editors). Reviews in Mineralogy and Geochemistry **67**, Mineralogical Society of America, Chantilly, VA, and the Geochemical Society, Washington, D.C.

Papike, J.J., Ross, M. and Clarke, J.R. (1969) Crystal chemical characterization of clinoamphiboles based on five new structure refinements. *Mineralogical Society of America Special Paper*, **2**, 117–136.

Popp, R.K., Virgo, D., Yoder, H.S. Jr., Hoering, T.C. and Phillips, M.W. (1995) An experimental study of phase equilibria and Fe oxy-component in kaersutitic amphibole: implications for the f_{H_2} and a_{H_2O} in the upper mantle. *American Mineralogist*, **80**, 534–548.

Popp, R.K., Hibbert, H.A. and Lamb, W.M. (2006) Oxy-amphibole equilibria in Ti-bearing calcic amphiboles: Experimental investigation and petrologic implications for mantle-derived amphiboles. *American Mineralogist*, **91**, 54–66.

Pouchou, J.L. and Pichoir, F. (1985) 'PAP' $\varphi(\rho Z)$ procedure for improved quantitative microanalysis. *Microbeam Analysis*, **1985**, 104–106.

Robinson, K., Gibbs, G.V., Ribbe, P.H. and Hall, M.R. (1973) Cation distributions in three hornblendes. *American Journal of Science*, **273A**, 522–535.

Schumacher, J.C. (2007) Metamorphic amphiboles: composition and coexistence. Pp. 359–416 in: *Amphiboles: Crystal Chemistry, Occurrence, and Health Issues* (F.C. Hawthorne, R. Oberti, G. Della Ventura and A. Mottana, editors). Reviews in Mineralogy and Geochemistry **67**, Mineralogical Society of America, Chantilly, VA, and the Geochemical Society, Washington, D.C.

Shannon, R.D. (1976) Revised effective ionic radii and systematic studies of interatomic distances in halides and chalcogenides. *Acta Crystallographica*, **A32**, 751–767.

Sheldrick, G.M. (1998) *SADABS User Guide*, University of Göttingen, Germany.

van Aken, P.A. and Liebscher, B. (2002) Quantification of ferrous/ferric ratios in minerals: new evaluation schemes of Fe L_{23} electron energy-loss near-edge spectra. *Physics and Chemistry of Minerals*, **29**, 188–200.

van Aken, P.A., Liebscher, B. and Styrsa, V.J. (1998) Quantitative determination of iron oxidation states in minerals using Fe $L_{2,3}$-edge electron energy-loss near-edge structure spectroscopy. *Physics and Chemistry of Minerals*, **25**, 323–327.

van Alboom, A. and De Grave, E. (1996) Temperature dependence of the ^{57}Fe Mossbauer parameters in riebeckite. *Physics and Chemistry of Minerals*, **23**, 377–386.